ROMANIAN ACADEMY
School of Advanced Studies of the Romanian Academy
"Petru Poni" Institute of Macromolecular Chemistry from Iași

SUMMARY OF DOCTORAL THESIS

NEW ECOLOGICAL MATERIALS BASED ON NATURAL POLYMERS

PhD SUPERVISOR,

CS I Dr. Habil. Iuliana Spiridon

PhD STUDENT,

Irina Pop (married Apostol)

Iași
2023

ACKNOWLEDGEMENTS

I would like to thank to all encouraged me throughout this important stage of my life.

I would like to express my grateful to Dr. Habil. Iuliana Spiridon for the support she has provided me during this journey. Our collaboration has been a constant source of inspiration for me.

Sincere thanks to the members of the guidance committee, Dr. Narcis Anghel, Dr. Mirela Fernanda Zaltariov, and Dr. Maria-Valentina Dinu, for the suggestions and support offered during my doctoral studies.

I want to extend my thanks to the jury commission, Prof. Dr. Alexandra-Raluca Iordan, Prof. Dr. Teodor Măluțan, and CS I Dr. Dan Roşu, for their kindness in evaluating the content of the thesis and for the valuable suggestions provided.

I am grateful to my colleagues from Laboratory of Natural Polymers, Bioactive and Biocompatible Materials, and those from "Petru Poni" Institute of Macromolecular Chemistry from Iași for their advices and collaboration.

Thanks to the Romanian Academy for the financial support provided and to the board of the "Petru Poni" Institute of Macromolecular Chemistry from Iași for the opportunity to work within a high-quality learning environment.

I would like to express my profound thanks to my parents for their unwavering support.

I want to thank my husband, Vlad, for his patience, trust, and support.

Thank you!

Table of content

ABBREVIATIONS

Asp – aspartic acid; **BF** – basic fuchsine ; **CF** – cobalt ferrite; **CFLB** – cobalt ferrite – Lignoboost hybrid; **CFLO** – cobalt ferrite – organic lignin hybrid; **CL** – montmorillonite; **DLS** – dynamic light scattering; **DMF** – dimethylformamide; **XRD** – X–ray diffraction; **DVS** – dynamic vapor sorption; **BET equation** –Brunauer-Emmett-Teller equation; **EDX** – Energy-dispersive X-ray spectroscopy; **FTIR** – Fourier-transform infrared spectroscopy; **Glu** –glutamic acid; **LB** –Lignoboost lignin; **LBOL** – Lignoboost esterified with oleic acid; **LBST** – Lignoboost esterified with stearic acid; **MB** – methyl blue; **Oh** – octahedral; **PFO** – pseudo first order reaction; **PSO** – pseudo second order reaction; **PZC** – point of zero charge; **NMR** – nuclear magnetic resonance; **SEM** – scanning electron microscopy; **Ser** – serine; **Th** – tetrahedral; **UV–Vis** – ultraviolet/visible; **XG** – xanthan gum; **XGAC** – xanthan gum esterified with acrylic acid; **XPS** – X-ray photoelectron spectroscopy.

INTRODUCTION

Water pollution with organic dyes or oils is caused by the release or leakage of waste from various industries such as textile, food, pharmaceutical, or petrochemical. The presence of these pollutants in wastewaters has disrupted the entire aquatic ecosystem. As a result, researchers have been concerned with the "collection" of these wastes through environmentally friendly methods. It has been concluded that the use of materials with adsorptive properties represents a viable solution.

Natural polymers, such as lignin or xanthan gum, represent a promising alternative for the development of new adsorptive materials. They offer a series of advantages (biocompatibility, low cost, biodegradability etc.) that could contribute to improving the quality of life. Lignin has been utilized as a *source of new hybrid materials*. Furthermore, through enzymatic esterification – *one of the very first approaches in lignin chemistry* – compounds with interesting properties were synthesized and subsequently incorporated into xanthan-based matrices. Xanthan gum was esterified through the reaction with acrylic acid, and its ester, used as a matrix, facilitated the *development of new materials with potential applications*.

Achieving climate goals and transitioning to circularity through the utilization of sustainable materials represent one of the challenges faced by contemporary society.

The doctoral thesis **"New ecological materials based on natural polymers"** contributes to the field of research related to the utilization of natural polymers in the development of new materials using environmentally friendly methods.

The **general objective** of the thesis was **the development of new materials based on natural polymers with adsorptive properties for the treatment of wastewaters**. The studies were focused on the obtaining of new materials, their characterization, and testing in environmental applications.

The research within the doctoral thesis aimed to achieve several **specific objectives**:

O1. Esterification reactions of xanthan gum and lignin using methods that limit the use of environmentally harmful solvents; **O2.** Proposing an alternative way for the esterification of lignin and xanthan gum; **O3.** Synthesizing cobalt ferrite and cobalt ferrite-lignin hybrids for incorporation into polymeric matrices to enhance the adsorption capacity of the final materials; **O4.** Producing new materials with adsorptive properties and characterizing them through a series of specific analyses (FTIR, XRD, XPS, PZC, DVS,

DLS, SEM, EDX); **O5.** Testing the adsorptive properties of the materials (identifying adsorption capacity for anionic/cationic dyes and degraded oils) and conducting kinetic, thermodynamic, and equilibrium isotherm studies.

The thesis is structured in two parts:

Part I presents the current state of research regarding the use of materials with adsorptive properties and the main characterization methods used in the experiments covered by the thesis. The literature review includes the following chapters:

Chapter 1 describes the negative effects of water pollution and the materials used in the adsorption processes of pollutants. It also provides a brief overview of adsorption processes, including kinetic, thermodynamic, and equilibrium isotherms studies.

Chapter 2 includes a brief review of the main techniques and analysis methods of the studied compounds/materials.

Part II is organized into 6 chapters and includes the original results.

Chapter 3 presents the preparation, characterization, and the adsorptive properties of the materials based on xanthan gum or esterified xanthan gum and cobalt ferrite.

Chapter 4 is dedicated to the synthesis of cobalt ferrite-lignin hybrids. These hybrids were subsequently characterized to determine their physico-chemical properties and potential applications.

Chapter 5 describes the obtainment of new materials by incorporating cobalt ferrite-lignin hybrids into xanthan gum or esterified xanthan gum matrices. The resulting systems were characterized and tested for their ability to retain certain dyes.

Chapter 6 highlights the enzymatic esterification reaction of Lignoboost lignin with two fatty acids (stearic acid and oleic acid), which represents one of the very first approaches to this type of lignin chemistry. The obtained esters were characterized to confirm structural modifications.

Chapter 7 presents the development of new systems containing lignin esters. These materials were used in studies for the retention of degraded oils from wastewaters.

Chapter 8 details aspects related to the influence of montmorillonite on the properties of materials containing lignin esters. The systems were characterized and tested for the adsorption of degraded oils from wastewaters.

PART II. ORIGINAL CONTRIBUTION

CHAPTER 3

MATERIALS BASED ON XANTHAN GUM AND FERRITE. ADSORPTIVE PROPERTIES

In this chapter were developed new adsorptive materials based on XG, XGAC and CF.

3.1. Materials obtainment

The esterification reaction of XG with acrylic acid (**Scheme 1**) was carried out to reduce its hydrophilic character. The mixture of methylene chloride, tosyl chloride, acrylic acid, and pyridine was stirred continuously at reflux for 60 minutes. Pyridine hydrochloride (py·HCl), formed as a by-product, was removed by filtration. In the next step, XG was added to the filtrate, and the mixture was stirred for 24 hours at room temperature. The resulting product (XGAC) was separated by vacuum filtration, washed with methylene chloride and ethanol, and dried at room temperature (Anghel et al., 2021).

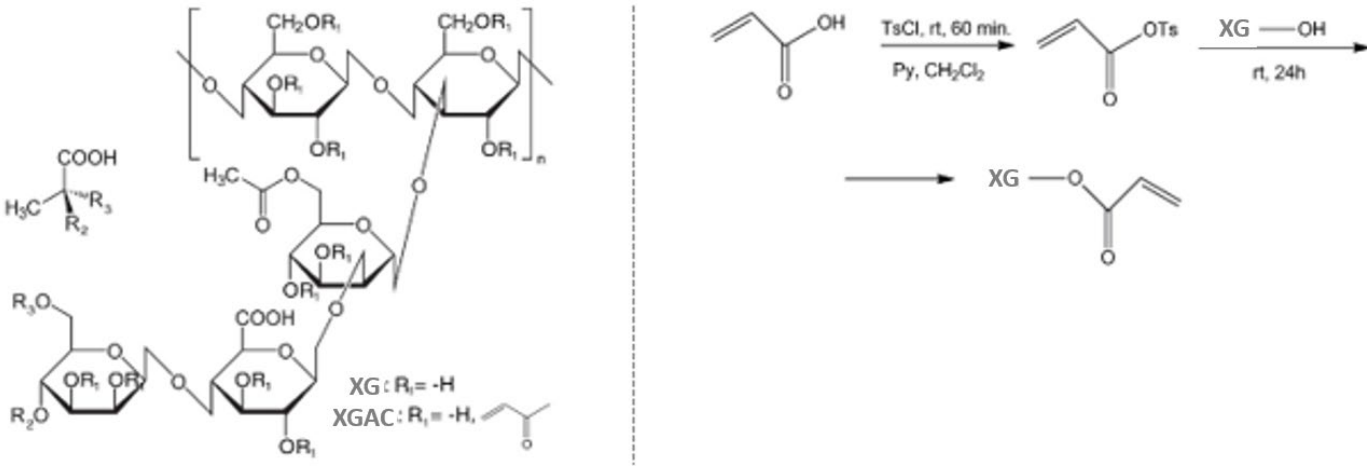

Scheme 1. Structural differences between XG and XGAC molecules; esterification reaction steps of XG with acrylic acid

CF was obtained through the co-precipitation method, following the steps presented in **Scheme 2**.

The preparation of absorptive materials (XGCF and XGACCF) was accomplished by incorporating CF into 0.5% solutions of XG and XGAC. The mixtures were poured into Petri dishes and dried at 60°C.

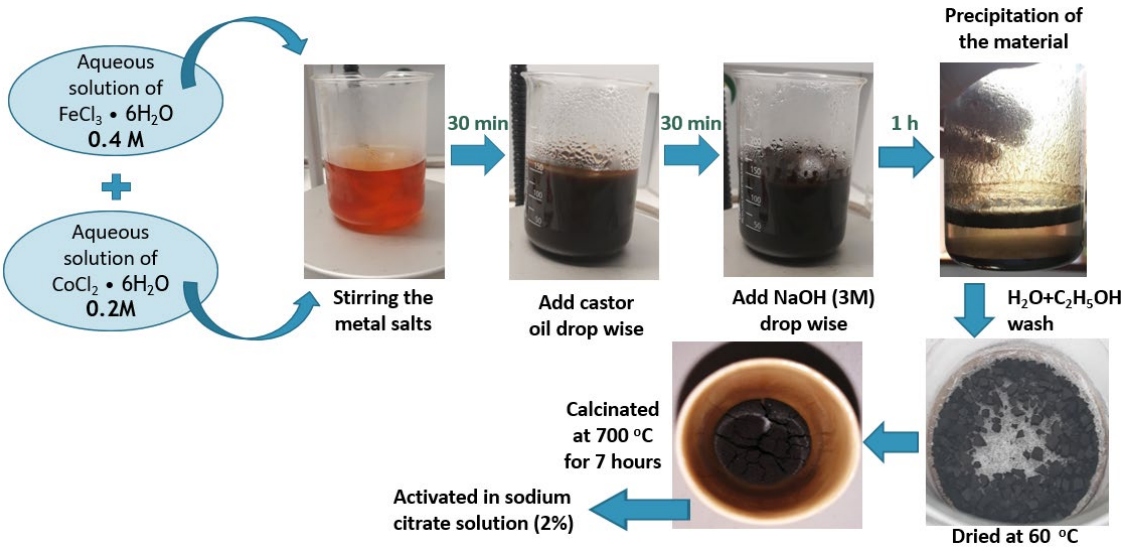

Scheme 2. Scheme for the synthesis of CF *via* co-precipitation method

3.2. Materials characterization

^{1}H-NMR spectroscopy

In **Figure 1** are presented ^{1}H–RMN spectra of XG and XGAC.

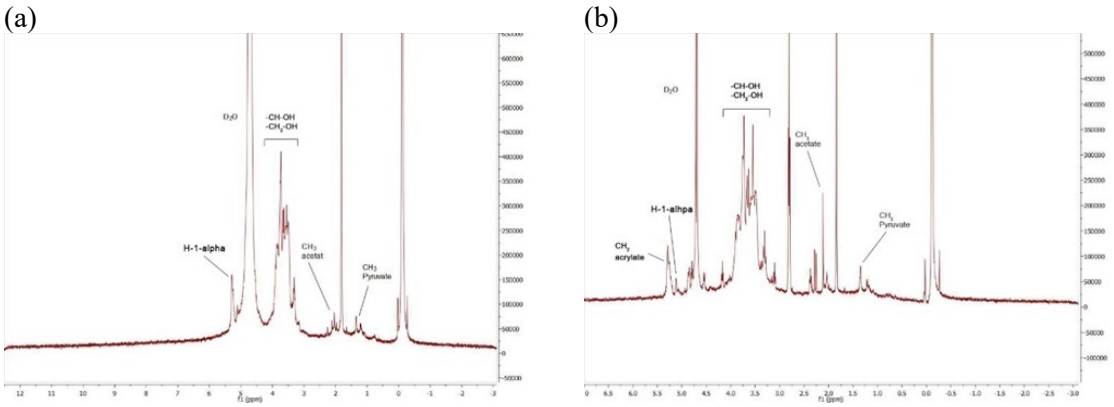

Figure 1. ^{1}H–NMR spectra of (a) XG and (b) XGAC

The success of the chemical modification of XG is confirmed by the ^{1}H–NMR spectrum of XGAC, which shows a signal at 5.5 ppm, characteristic of the beta protons in the acrylic group (Anghel et al., 2021). The introduction of a new ester group into the structure of XG is further confirmed by FTIR spectroscopy. The spectra (**Figure 2**) demonstrate the increase of the intensity for the absorption band at 1720 cm^{-1} (corresponding to the carbonyl group). The signals from 1488 cm^{-1} and 919 cm^{-1} confirm the presence of C=C double bonds (Anghel et al., 2021).

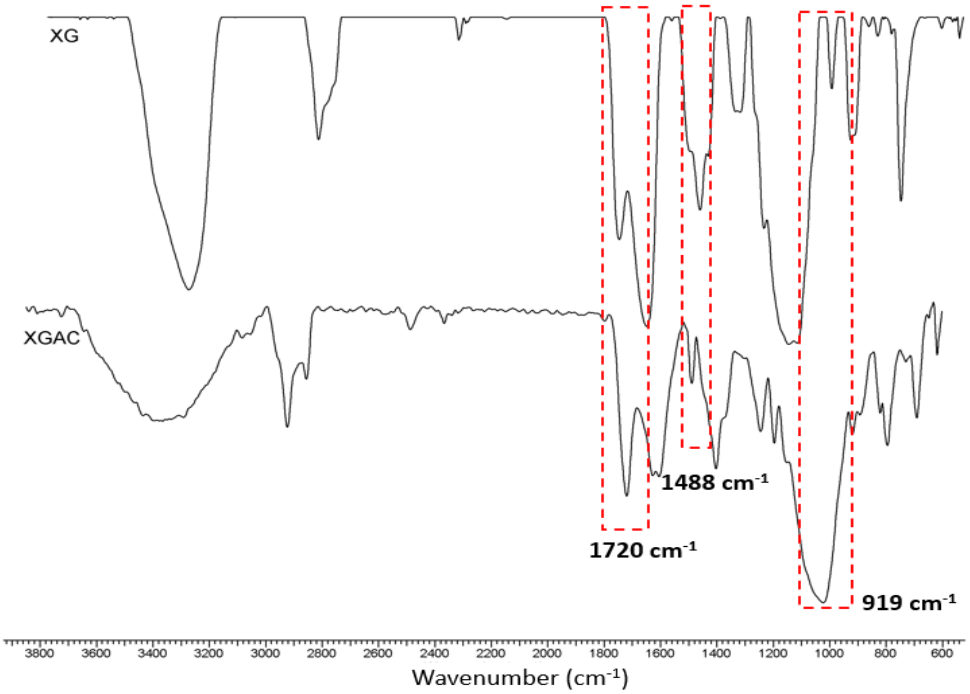

Figure 2. FTIR spectra of XG and XGAC

The materials were characterized using XRD, which confirmed the presence of ferrite within the polymeric matrices. SEM images revealed ferrite particles as polydisperse mesoporous aggregates. XG and XGAC appeared as homogeneous materials. Images of XGCF and XGACCF highlighted the dispersion of inorganic particles within the polymeric matrix.

The capacity for water vapor sorption

DVS analysis indicates that the presence of CF in XGCF and XGACCF materials determines a decrease of the specific surface with approximately 40%, as compared with those of XG and XGAC (**Table 1**). This led to more dense materials due to the electrostatics interactions.

Table 1. DVS parameters

Sample	Sorption capacity, % d.b.	Area, $m^2 \times g^{-1}$	Monolayer, $g \times g^{-1}$
XG	47.78	415.8	0.118
XGCF	44.06	299.5	0.085
XGAC	49.22	498.3	0.141
XGACCF	42.31	278.2	0.079
CF	1.17	0.106	3×10^{-4}

3.3. Dyes retention from wastewaters

In this study, the retention of MB and BF from aqueous solutions was investigated.

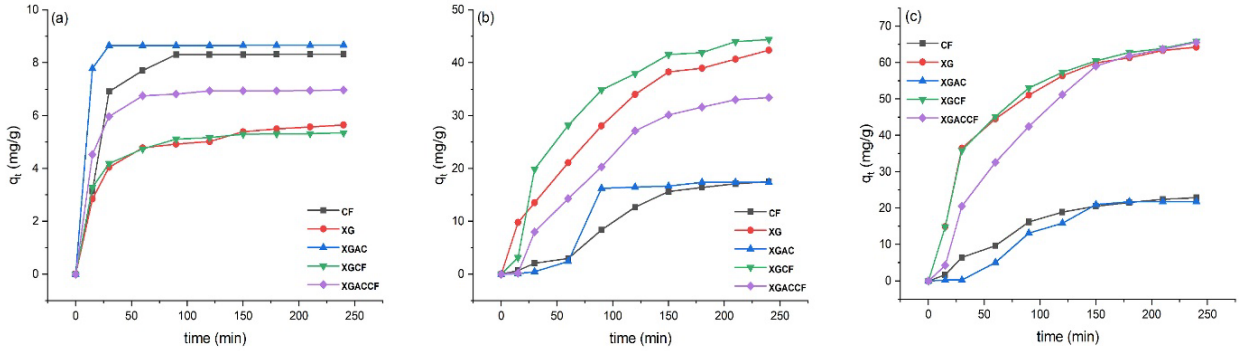

Figure 3. Effect of contact time on MB adsorption capacity at different concentration: (a) 10 mg/L, (b) 50 mg/L and (c) 70 mg/L

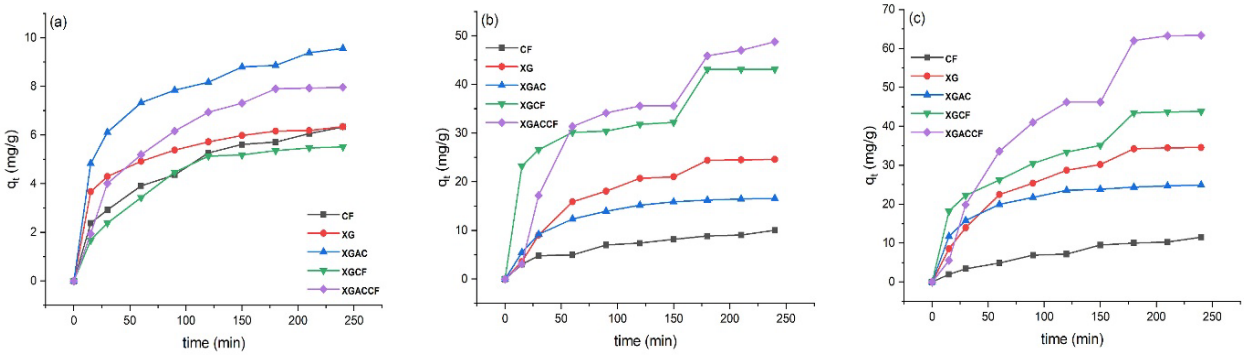

Figure 4. Effect of contact time on BF adsorption capacity at different concentration: (a) 10 mg/L, (b) 50 mg/L and (c) 70 mg/L

Adsorption was efficient within the first ~50 minutes for all dye solutions (**Figures 3** and **4**). XGACCF shows the highest value for q_t (mg/g) in retaining BF (63.35 mg/g). The highest value for q_t (mg/g) in MB adsorption process is recorded upon use XGCF (65.84 mg/g) (Spiridon et al., 2022).

Kinetic study

The experimental data were analyzed using three kinetic models: PFO, PSO and Elovich. The R^2 value determined from the PSO model ($R^2 > 0.9384$) for BF adsorption is higher than that obtained with the PFO model ($R^2 > 0.7597$). Some authors suggest an exchange of electrons between the groups in the dye molecule and those in the polymeric material structure (Tian et al., 2020; Wei et al., 2021). In the case of MB adsorption, according to PFO model, R^2 values range from 0.8467 to 0.9944, and the q_e (cal) values are

close to those calculated based on this model (q_e (exp)). The correlation with this kinetic model highlights the physical nature of the process (Chandarana et al., 2021).

Adsorption isotherms study

The experimental data were evaluated using the Langmuir, Freundlich, Dubinin-Radushkevich, Temkin, and Jovanović models. The adsorption equilibrium of MB and BF on CF and XGAC is best described by the Langmuir model (R^2 values ranging from 0.9260 to 0.9884) (Bendini et al., 2007). The surfaces of CF and XGAC materials are covered with a layer of dye molecules. The adsorption equilibrium of the dyes on XG, XGCF, and XGACCF materials is described by Dubinin-Radushkevich model. R^2 values range from 0.9124 to 0.9996, and $q_{max\ D\text{-}R}$ values are close to the maximum adsorption capacity determined experimentally. These results suggest that the process is correlated with the filling of micropore volume (Hu et al., 2019).

Thermodynamic study

The effect of temperature on the adsorption capacity of the materials was investigated at 25, 35, and 45°C for dye solutions with a concentration of 10 mg/L. **Figure 4** shows the graphical representations of the Van't Hoff equation using the experimental data.

According to the obtained results, it has been revealed that the adsorption process of both dyes was exothermic (Wang et al., 2020).

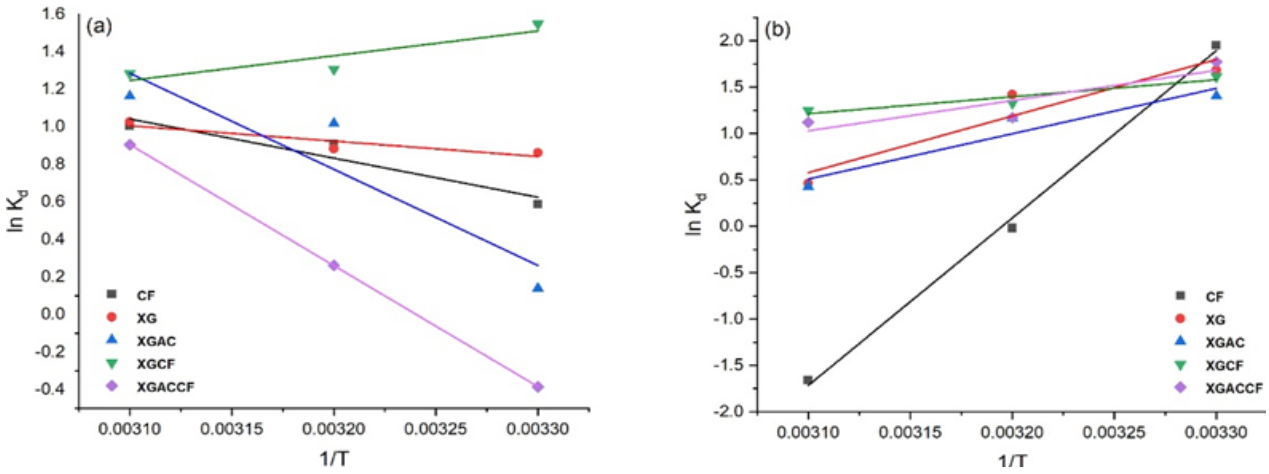

Figure 4. Van't Hoff's plot for the sorption of (a) MB and (b) BF onto studied materials

CHAPTER 4

SYNTHESIS AND CHARACTERIZAION OF COBALT FERRITE–LIGNIN HYBRIDS

In this study, lignin was used as a source for the development of new hybrid materials. The compounds were obtained through an environmentally friendly and cost-effective method.

4.1. Hybrid materials obtainment

The CF-lignin hybrids were obtained through the sol-gel method, following the steps presented in **Scheme 3**.

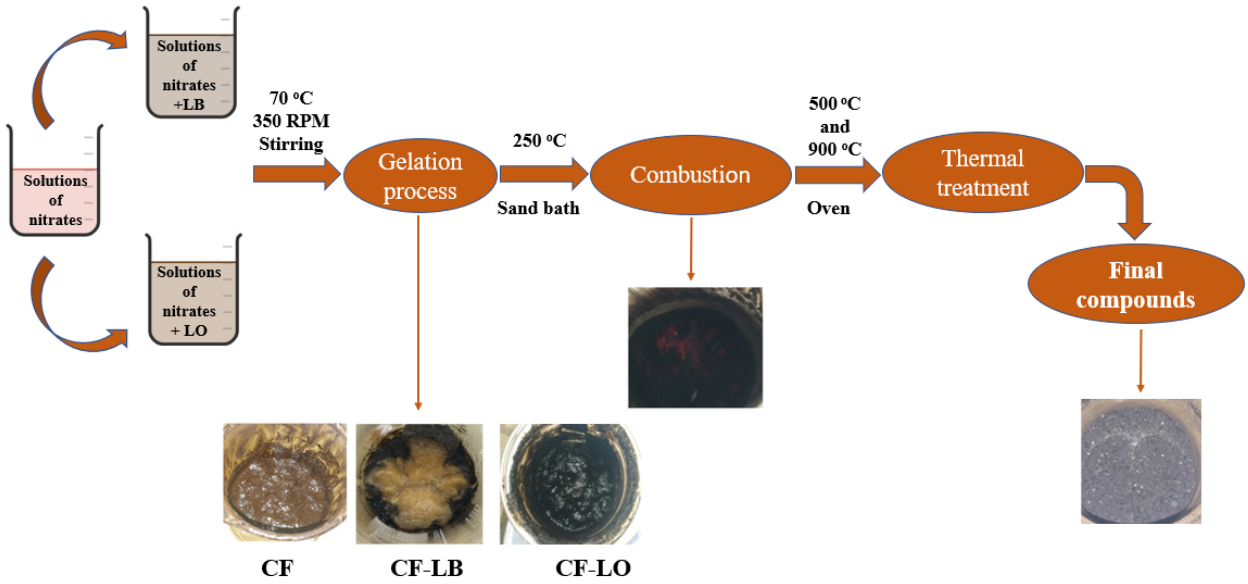

Scheme 3. Schematic illustration of the ferrite–lignin hybrids obtainment

LO and LB replaced the commonly used combustion-complexing agents (such as citric acid or glycine). This approach allowed the utilization of lignin, which is a by-product from pulp and paper industry. Iron nitrate ($Fe(NO_3)_3 \cdot 9H_2O$) and cobalt nitrate ($Co(NO_3)_2 \cdot 6H_2O$) were used as source of cations.

The samples were named according to the combustion-complexing agent used and the temperature, as follows: CF-LB500, CF-LB900, CF-LO500, CF-LO900.

4.2. Hybrids characterization

FTIR spectroscopy

Figure 5 presents the FTIR spectra of the hybrids and the lignins used as combustion-complexing agents. The IR analysis confirms the formation of CF-lignin hybrids.

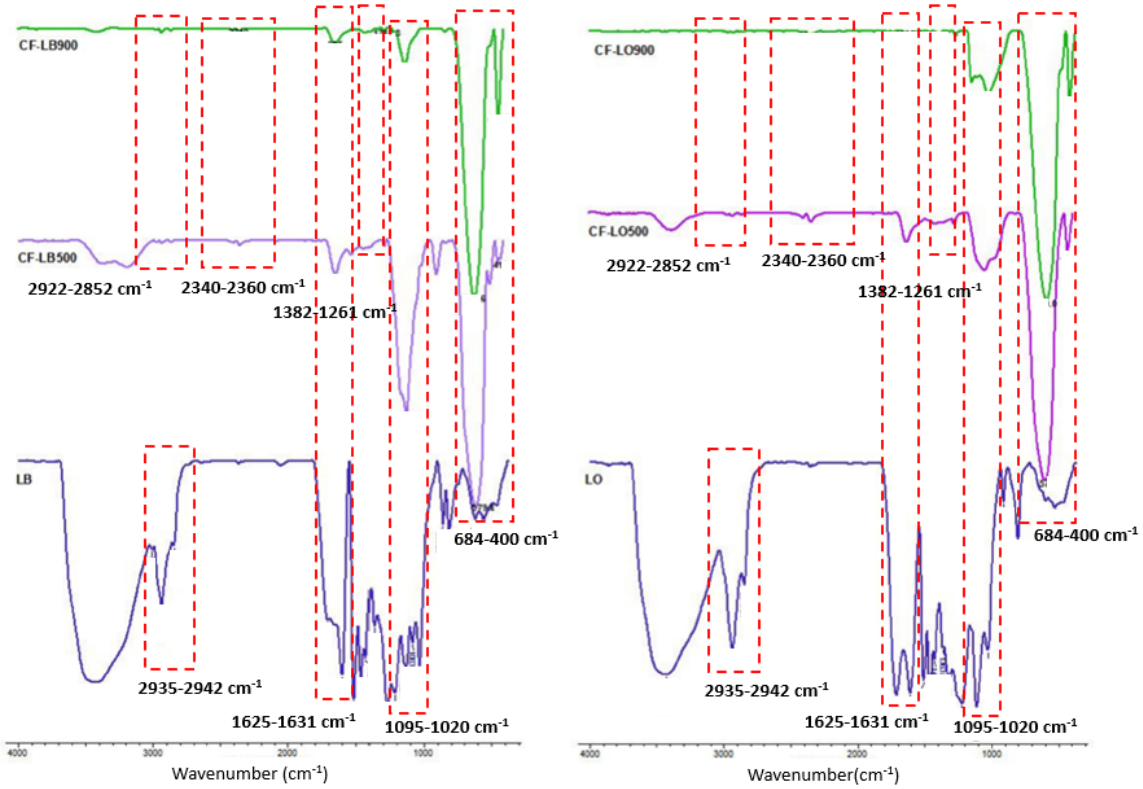

Figure 5. FTIR spectra of CF–lignin hybrids

The absorption bands present at 684 cm^{-1} and 400 cm^{-1} were due to the stretching vibrations of metal oxide in the Oh group complex Co (II)–O^{2-} and Fe (III)–O^{2-} Th group complex of the cobalt ferrite phase, respectively. An important peak at 1382 cm^{-1}, which can be attributed to aliphatic C–H in the methyl groups, was also recorded for the hybrid materials, as well as the peak at 1261 cm^{-1}, specific to G ring. The peaks at 1095 cm^{-1} and 1020 cm^{-1}, specific to the aromatic C-H deformation of S units and the C–O deformations of secondary alcohols and aliphatic ethers aromatic C-H in-plane deformation presented in the spectra of hybrids (Damacena et al., 2019), also indicate the presence of the organic component (lignin) in the analyzed materials.

The crystallinity of hybrids

XRD diffractograms of hybrid materials are presented in **Figure 6**.

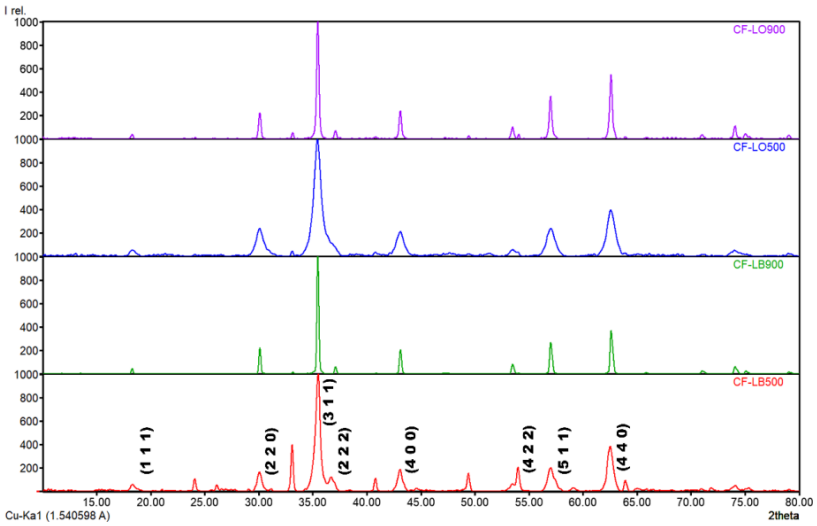

Figure 6. XRD spectra of lignin hybrids

The two-theta values (30.08, 35.43, 37.05, 43.05, 53.44, 56.9, and 62.58) corresponding to the reflections of (220), (311), (222), (400), (422), (511), and (440) planes, confirm the formation of cobalt ferrite-based materials with a spinel structure. Compared to the hybrids obtained at 500°C, those treated at 900°C exhibit much sharper and narrower peaks, indicating an increased crystallinity as a result of atomic arrangement with the rise in calcination temperature.

X-ray photoelectron spectroscopy

XPS spectra of hybrid materials are presented in **Figure 7**.

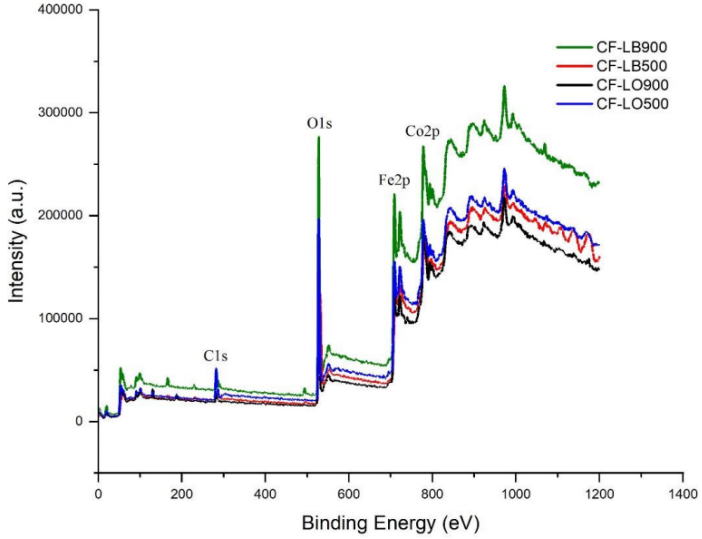

Figure 7. XPS spectra of ferrite-lignin hybrids

The binding energies at about 780.1 eV, 710.7 eV, 529.8 eV, and 284.7 eV, which are attributed to the core photoionization signals of Co 2p, Fe 2p, O 1s, and C 1s, respectively, represent a clear proof of the successful synthesis of ferrite-lignin hybrids. The relative height peak of the C1s at 284.7 eV confirms the presence of carbon in all materials.

Particles size distribution

All hybrid's suspensions were relatively monodispersed; the analysis indicated the presence of a unimodal size distribution (**Figure 9**) with polydispersity indices of 1.00 for CF-LO900 and 0.539 for CF-LO500. The hybrids comprising organic lignin recorded closer values, as follows: 0.968 for CF-LB900 and 0.598 for CF-LB500. The increase in the polydispersity indices with the increase in calcination temperature shows good stabilization of the ferrite-lignin particles.

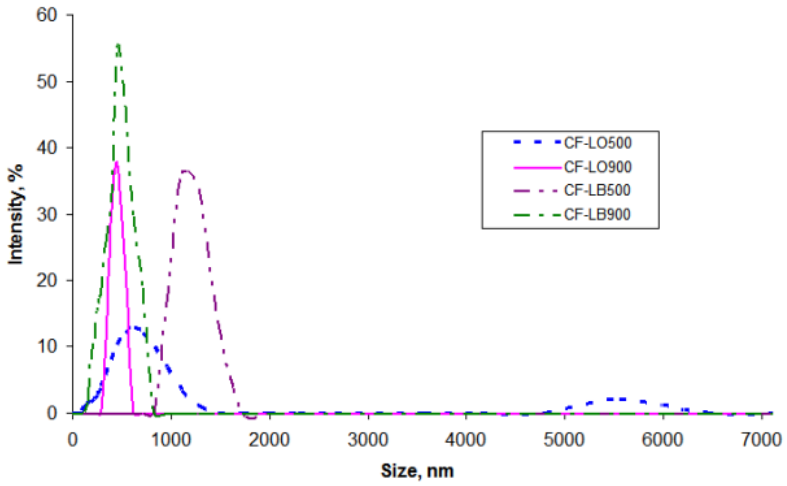

Figure 8. The distribution of particles size for the ferrite-lignin hybrids

CHAPTER 5

MATERIALS BASED ON XANTHAN GUM AND COBALT FERRITE–LIGNIN HYBRIDS. ADSORPTIVE PROPERTIES

Materials based on XG or XGAC and CF-lignin hybrids were developed and used for the removal of MB and BF dyes from wastewaters.

Materials based on XG and CF-lignin hybrids were prepared by incorporating hybrids obtained at 500°C into 0.5% solutions of XG and XGAC, respectively. The choice of hybrids is justified by their high specific surface area and superior sorption capacity

compared to those obtained at 900°C. The materials were named based on the polymeric matrix and the hybrid introduced into it, as follows: XG/CFLB, XG/CFLO, XGAC/CFLB, XGAC/CFLO.

5.1. Materials characterization

The sorption capacity for water vapors

The data presented in **Table 2** show that the nature of the polymeric matrix influences water sorption capacity. Materials based on XGAC have a lower sorption capacity compared to those containing XG. Through esterification, xanthan becomes more hydrophobic, thus allowing the establishment of intra- and intermolecular interactions between polymeric chains through London dispersion forces.

Table 2. DVS parameters

Sample	Sorption capacity, % d.b.	Area, m^2/g	Monolayer, g/g
XG/CFLB	45.70	273.5	0.078
XGAC/CFLB	39.60	253.4	0.072
XG/CFLO	47.80	297.4	0.084
XGAC/CFLO	42.60	301.4	0.085

Point of zero charge

Table 3 presents the PZC values for the materials. The pH of the dye solutions was not adjusted and ranged from 6.0 to 6.5. According to our data, CFLO and XG/CFLB materials present $pH < pH_{PZC}$ and are suitable for MB (anionic dye) retention. CFLB, XG/CFLO, XGAC/CFLB and XGAC/CFLO materials presented values of $pH \geq pH_{PZC}$. Therefore, they seem to be more suitable for BF (cationic dye) adsorption.

Table 3. Determined PZC values

Material	PZC
CFLB	5.80
CFLO	7.00
XG/CFLB	7.80
XG/CFLO	6.10
XGAC/CFLB	6.25
XGAC/CFLO	6.05

5.2. Dyes retention from wastewaters

The adsorption tests were performed on solutions of MB and BF with concentrations of 15, 50, and 70 mg/L. CFLB, CFLO, and XG/CFLO retained the highest amounts of MB dye (44.73, 37.54, and 24.54 mg/g, respectively). XG/CFLO, XG/CFLB, and XGAC/CFLO demonstrated the best adsorption capacity for BF dye (36.23, 33.33, and 31.34 mg/g, respectively).

Kinetic study

The experimental data were correlated with three different models (PFO, PSO, and Elovich). R^2 values ranging from 0.931 to 1.000 demonstrate that the adsorption process correlates with the PSO model. Additionally, the q_e (cal) values are nearly equal to the experimental ones. Data from the literature suggest the establishment of interactions involving electron exchange between the groups in the structure of dye molecules and those of the materials (Wei et al., 2021). For most systems, a decrease in the rate constant k_2 was observed as the concentration increases from 15 to 70 mg/L. These results are attributed to the intensified competition among dye molecules for the material surface.

Adsorption isotherms study

The results were evaluated using the Langmuir, Freundlich, Dubinin-Radushkevich, Temkin, and Jovanović models. For MB adsorption, the experimental results obtained for CFLB, CFLO, XG/CFLB, XG/CFLO, and XGAC/CFLB are correlated with the Langmuir model (R^2 values range from 0.845 to 1.000). The q_{max} values (mg/g) calculated according to the Langmuir model (47.89, 35.77, 10.76, 24.80, and 20.53 mg/g) are close to the experimental values (44.73, 37.54, 9.58, 24.54, and 17.15 mg/g). In the case of XGAC/CFLO material, the experimental data for MB adsorption correlates with the Jovanović model ($R^2 = 0.963$). According to this model, the dye is deposited in a monolayer on the material (Ramadoss et al., 2019). The experimentally determined q_{max} value (8.60 mg/g) is close to the theoretically obtained value (8.69 mg/g). For BF dye adsorption, the experimental results obtained for XG/CFLB, XG/CFLO, XGAC/CFLB, and XGAC/CFLO materials correlate with the Dubinin-Radushkevich model (R^2 values range from 0.942 to 0.997), that assumes the deposition of dye molecules throughout the micropore volume. CFLB and CFLO materials resonates more with the Jovanović model.

CF–lignin hybrids reusability

The addition of ferrite-lignin hybrids into materials has improved their properties in terms of reusability. Both hybrids maintain nearly the same capacity for adsorbing the dye MB (**Figure 10**). The dye retention process is shorter when hybrid materials are used, the equilibrium being reached in approximately 20 minutes. Materials containing CFLB and CFLO can be easily removed from aqueous solutions.

It is worth noting that the CFLB hybrid retains an average of 90% of the dye, even after five cycles of use. This performance can be attributed to the large specific surface area, which allows the dye to be adsorbed into the material's pores. A sudden decrease in adsorption capacity is observed for CFLO, when tested on the 70 mg/L BF solution; this can be correlated with the material's positive charge at the pH levels used in the experiments (the PZC for CFLO is 7, so it retains anionic dyes in slightly acidic environments).

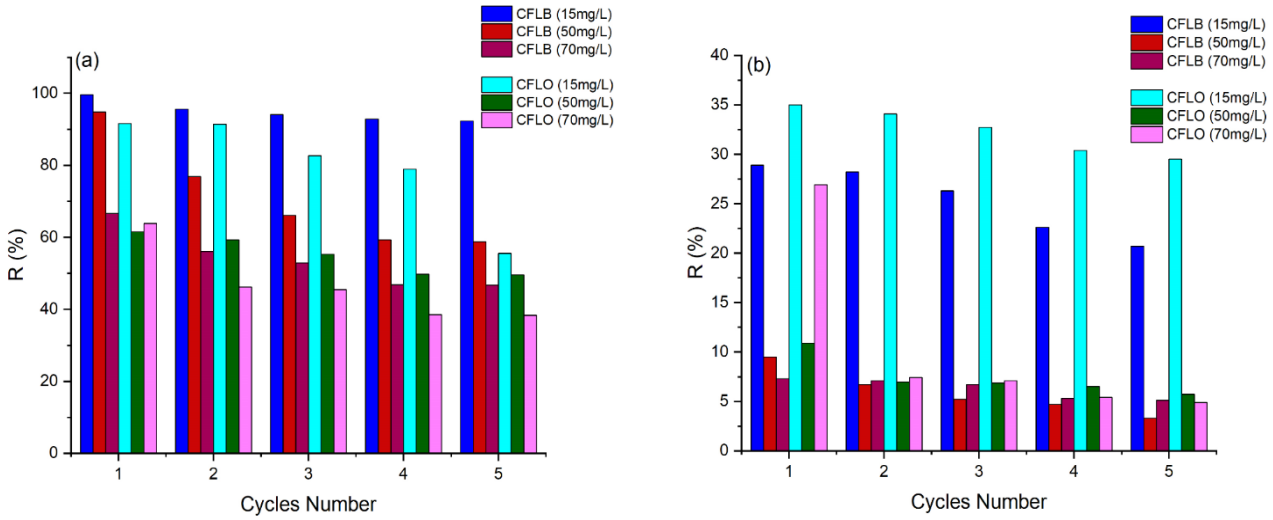

Figure 9. Dye adsorption capacity for (a) MB and (b) BF during five cycles using CFLB and CFLO adsorbents

Thermodynamic study

In **Table 4** are presented the values of the determined thermodynamic parameters. The enthalpy values are positive ($\Delta H^o > 0$) for all performed experiments, indicating the endothermic nature of the processes. The entropy values also show positive values ($\Delta S^o > 0$), indicating disorder at the interface between the solute and the material. The changes in experimental conditions led to modification of thermodynamic parameters. Thus, the temperature increase resulted in a decrease in ΔG^o. This aspect suggests that the adsorption

becomes spontaneous at higher temperatures. In these conditions, thermal agitation in the system accelerates the process (Sharma et al., 2013).

Table 4. Thermodynamic parameters for the removal of MB and BF by materials

Sample	Dye (15 mg/L)	ΔH^o (kJ/mol)	ΔS^o (kJ/mol×K)	ΔG^o (kJ/mol)		
				20 °C	30 °C	45 °C
CFLB	MB	94.79	0.034	-7.441	-13.930	-17.232
	BF	29.4	0.089	3.038	1.768	0.430
CFLO	MB	93.79	0.331	-3.265	-5.915	-17.198
	BF	29.88	0.094	1.744	1.207	-0.165
XG/CFLB	MB	127.13	0.439	-1.571	0.263	-15.949
	BF	20.11	0.061	1.292	0.937	-1.159
XG/CFLO	MB	34.10	0.147	-3.364	-10.882	-12.300
	BF	41.47	0.136	1.249	0.688	-1.759
XGAC/CFLB	MB	122.37	0.413	-9.466	-11.214	-13.936
	BF	24.05	0.076	1.091	-0.478	-3.016
XGAC/CFLO	MB	79.11	0.276	-2.792	-4.779	-11.462
	BF	33.21	0.108	1.014	-0.167	-2.278

CHAPTER 6

LIGNIN ENZYMATIC ESTERIFICATION. OBTAINMENT AND CHARACTERIZATION OF THE COMPOUNDS

This chapter is dedicated to the esterification reaction catalyzed by lipase, that represents one of the very first approaches in lignin chemistry. It is environmentally friendly, resulting in compounds with interesting properties. The obtained esters were characterized by different techniques (FTIR, ^{13}C-RMN and XPS spectroscopy).

6.1. Lignin enzymatic esterification

LB was esterified with two organic acids: oleic acid and stearic acid (**Scheme 4**).

The Ser-His-Asp/Glu triad forms the active site of lipases from various sources. A lipase-organic acid complex is created in this reaction pathway by the organic acid (acyl donor), first binding to the hydroxyl group of serine in the active site of the lipase through a nucleophilic attack. The subsequent conversion of the lipase-organic acid complex into an ester of organic acid with serine residue results in the simultaneous release of water. The second substrate, lignin, attacks this intermediate to create a serine-acyl-lignin complex. This complex separates into a lignin ester of organic acid (stearate – LBST or oleate – LBOL), and the enzyme reverts to its catalytically active state ready for the subsequent cycle of catalysis (Gandhi et al., 2000).

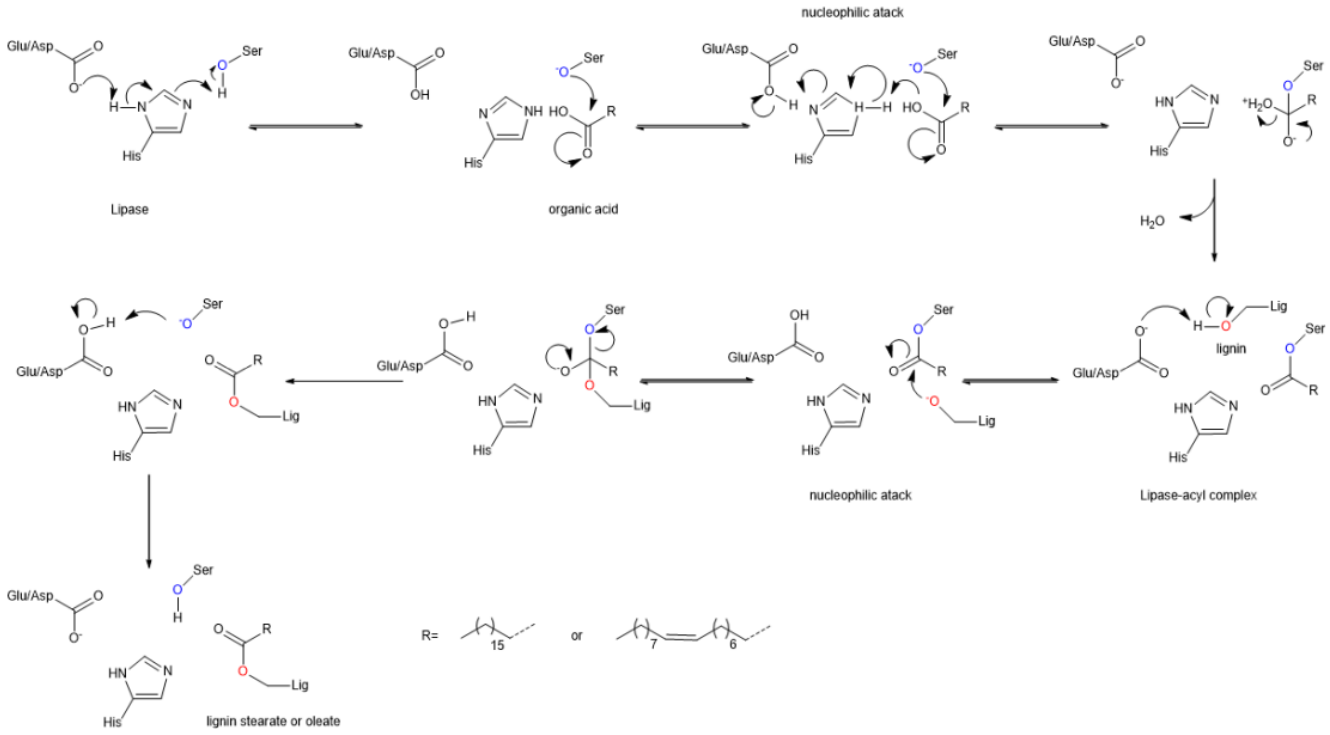

Scheme 4. Schematic representation of lipase-catalyzed esterification of lignin with organic acids

6.2. Lignin esters characterization

IR spectroscopy

FTIR spectra for LB and its esters are presented in **Figure 10**. A new peak at 1658.72 cm^{-1} characteristic of the C=C stretching vibrations from alkenes confirms that oleic acid was linked to the lignin macromolecule. The peaks associated with syringyl and guaiacyl groups (1269.1. 1213.1. 1141.82. 1124.46 cm^{-1}) have decreased in intensity in both LBOL and LBST spectra, while the signal around 1700 cm^{-1} characteristic of C=O group in esters increased, proving that the esterification has been successful. Also, the strong peaks at 2847 cm^{-1} and 2931 cm^{-1} attributed to long chain alkyl groups (aliphatic carbon) demonstrate lignin esterification (Yue et al., 2016).

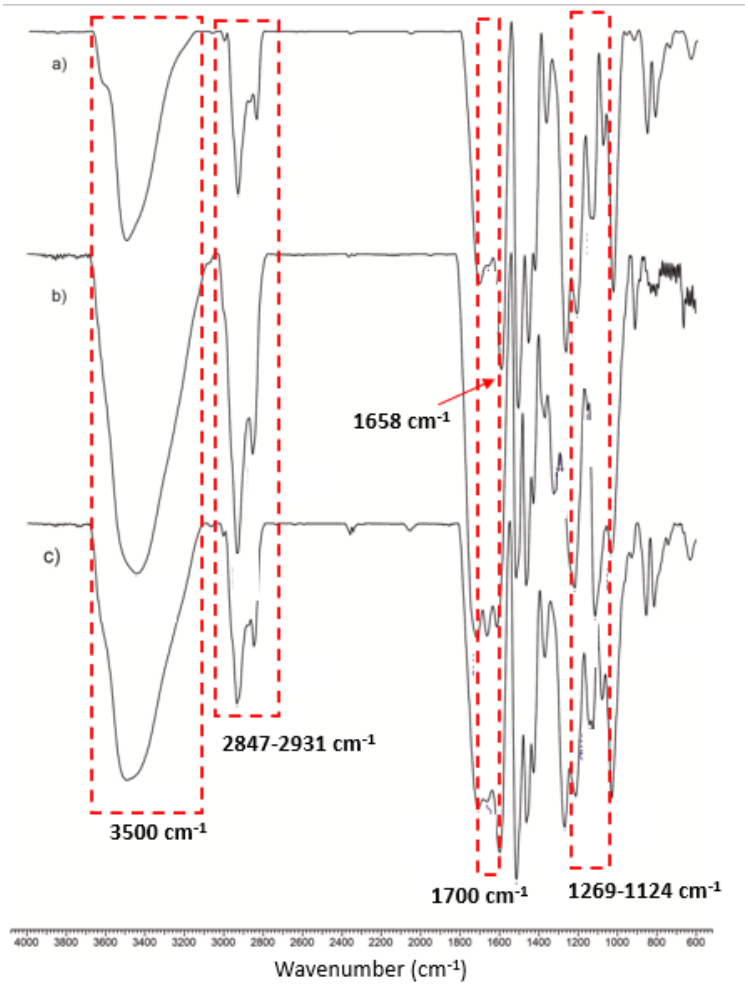

Figure 10. FTIR spectra of: a) LB, b) LBOL and c) LBST

^{13}C-RMN spectroscopy

The ^{13}C–NMR spectra of LB derivatives (**Figure 11**) present two peaks at 31.3 ppm and 25.4 ppm, assigned to aliphatic carbon atoms (Bridson et al., 2012) chains grafted onto the Lignoboost lignin molecules and prove the lignin esterification. Lignin derivatives present also some changes in the aliphatic carbon region (90 to 60 ppm), as well as in the interval 142–160 ppm due to esterified aromatic C atoms (Kocheva et al., 2011), confirming successful lignin modification.

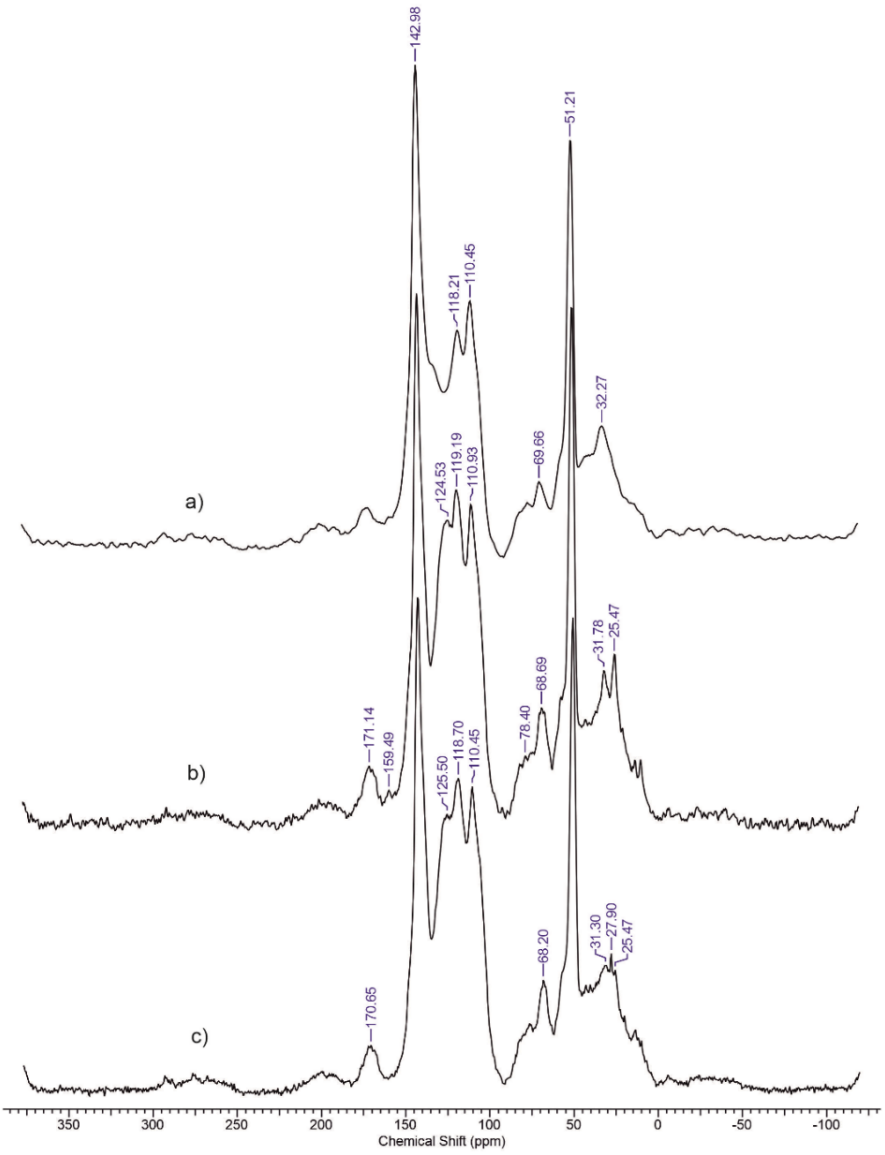

Figure 11. ^{13}C–NMR spectra of lignin and its derivatives: a) LB, b) LBOL and c) LBST

X-ray photoelectron spectroscopy

Spectral deconvolution was performed to identify the functional groups in LB, LBOL, and LBST. The C 1s spectra show signals at 284.6 eV, 285.0 eV, 286.18 eV, 287.5 eV and 289.3 eV, which are characteristic of the C=C, C–C, C–OH, C=O and O–C=O bonds in the lignin structure. According to the C 1s spectra of the esters, the content of C–OH bonds (286.5 eV) decrease as the number of C=O bonds increases. Deconvolution of the O 1s spectra revealed changes in the binding energy values for oxygen in the carbonyl group (531.4 eV), confirming the chemical modification of lignin.

Table 5 presents the elemental composition (the percentage values) for the studied compounds. The C/O ratio increases from 3.58 for LB to 3.62 (LBOL) and 3.69 (LBST). This change confirms the functionalization of the lignin surface.

Table 5. Chemical composition of analyzed samples

Element	Atomic concentration [%]		
	LB	LBOL	LBST
O	21.64	21.2	20.9
C	77.50	76.8	77.2
S	0.85	-	-
C/O	3.58	3.62	3.69

CHAPTER 7

MATERIALS BASED ON LIGNIN ESTERS. OILS ADSORPTION STUDIES

In this chapter, the capacity of materials containing XG and lignin esters to retain degraded oils from wastewater was investigated.

7.1. Materials obtainment

Scheme 4 describes the steps involved in the materials' obtainment.

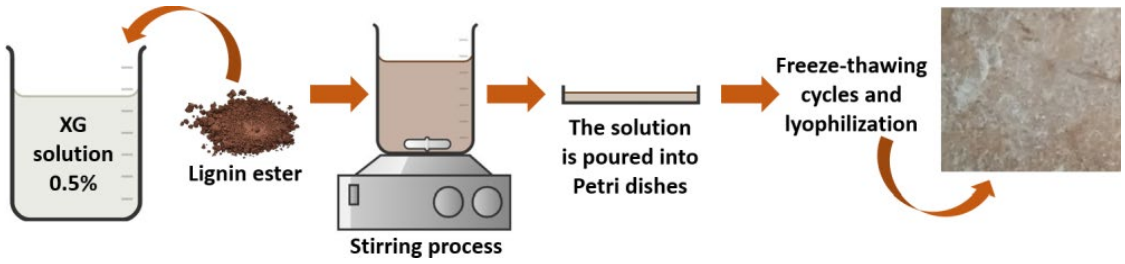

Scheme 4. Schematic illustration of materials preparation

7.2. Materials characterization

Compressive strength and materials morphology

The stress–strain (σ–ε) curves (**Figure 12B**) reveal an elastic behavior for all the samples. All the materials successfully sustained compression values beyond 78% (**Figure 12A**), without the appearance of network failure.

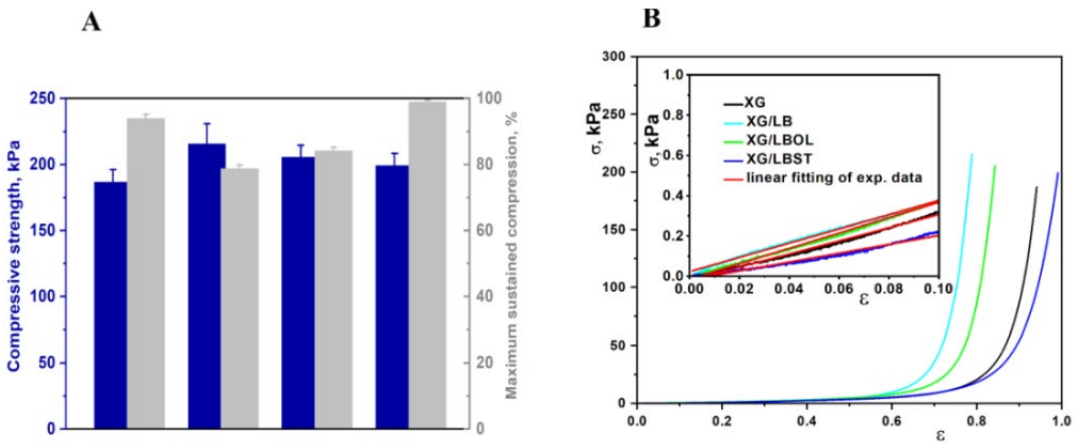

Figure 12. The mechanical properties of materials: A) Values of compressive nominal stress (dark blue columns) and of maximum sustained compression (grey columns); B) Stress-strain profiles (the inset presents the linear dependence of stress-strain profiles used to evaluate the compression elastic moduli);

All values were calculated as the average of at least three individual tests ± standard deviations.

The materials present pores with various shapes and sizes (**Figure 13**). Their morphology is heterogeneous.

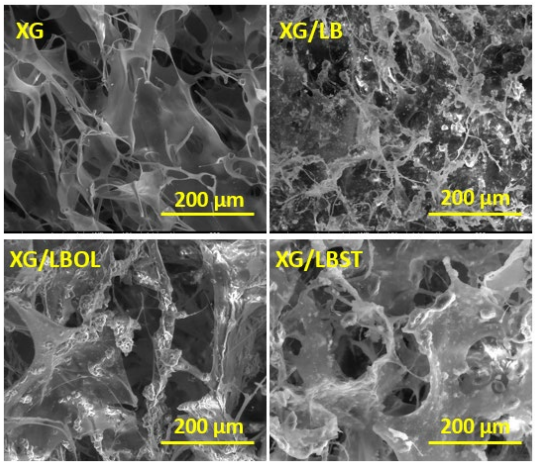

Figure 13. SEM images of materials

7.3. Oils adsorption studies

Retention tests for degraded argan and sunflower oils were conducted to assess the absorption capacity of materials containing XG and lignin esters.

In **Table 6** are presented the equilibrium adsorption capacities, q_e (g/g), for all the materials. Over 60% of the total oil quantity was adsorbed. The process reached the equilibrium after 120 seconds.

Table 6. Adsorption capacity values

Material	[a]q_e ± SD (g/g)					
	Argan oil			Sunflower oil		
	1 g	2 g	3 g	1 g	2 g	3 g
XG	42.58 ± 0.96	54.40 ± 1.52	61.19 ± 3.43	56.62 ± 1.65	59.23 ± 1.96	62.45 ± 2.93
XG/LB	42.62 ± 3.77	53.17 ± 1.73	55.14 ± 0.93	48.93 ± 4.90	53.56 ± 1.44	62.16 ± 3.96
XG/LBOL	34.76 ± 2.06	42.08 ± 0.90	43.39 ±2.64	43.20 ± 2.91	55.59 ± 2.19	51.95 ± 4.43
XG/LBST	37.46 ± 2.22	47.43 ± 1.91	53.02 ± 3.86	41.56 ± 3.10	44.62 ± 2.74	50.07 ± 1.86

[a] Data are expressed in the mean ± standard deviation (n = 3)

Argan oil is well retained by all the studied materials. XG, XG/LB and XG/LBST retained the highest quantities of this type of oil (61.19, 55.15 and 53.02 g/g). All the analyzed materials present equilibrium adsorption capacities of over 50 g/g for sunflower oil (62.45, 62.92, 51.95 and 50.07 g/g). These results can be attributed to the formation of secondary interactions (hydrogen bonds, van der Waals forces or π-π interactions) between the polymeric chains of the studied materials and the side chains of the degraded oil molecules (Guo et al., 2022).

Kinetic study

The experimental data correlates with the PSO model (R^2 ranging from 0.9814 to 1.0000). The PSO model theoretically describes chemical adsorption processes. Numerous studies have reported that this model is versatile and suitable for expressing the kinetics of physisorption processes and mass transfer/diffusion (Guo et al., 2022; Plazinski et al., 2009). FTIR spectra of oil-loaded materials were recorded and following the IR analysis, no signals suggesting the formation of new chemical bonds were identified. Therefore, it was concluded that the adsorption process of both oils is physical in nature.

Adsorption isotherms study

The experimental data were evaluated using the Henry, Langmuir, Freundlich, Temkin, and Harkin-Jura models. The adsorption equilibrium of argan oil on XG, XG/LB, and XG/LBOL materials is best described by the Langmuir model (with R^2 values ranging from 0.9894 to 1.0000). The experimental results for the XG/LBST system correlated with the Henry model ($R^2 = 0.9997$), which represents the simplest form of an adsorption isotherm and describes the process at lower adsorbate concentrations (Kalam et al., 2021). The adsorption equilibrium of sunflower oil data on XG/LBOL material are fitted on the Henry model ($R^2 = 0.9190$), while the adsorption equilibrium of sunflower oil on XG, XG/LB, and XG/LBST systems is described by the Harkin-Jura model (with R^2 values ranging from

0.9100 to 0.9999). The Harkin-Jura model is applicable to materials with heterogeneous surfaces and explains the adsorption in multiple layers of the adsorbate on the material surface (Saad et al., 2017).

SEM images of the oil-loaded materials are presented in **Figure 14**. It is noteworthy that, as a result of the adsorption experiments, the pores were completely occupied by oil molecules. These observations correlate with the pore filling behavior of the materials, as described by the adsorption isotherm models.

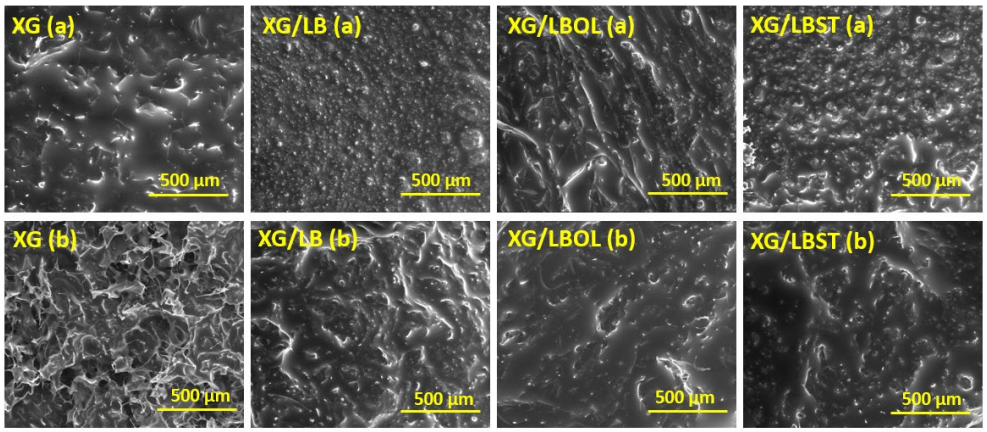

Figure 14. SEM images of materials loaded with (a) argan oil and (b) sunflower oil

CHAPTER 8

MONTMORILLONITE INFLUENCE ON ADSORPTIVE PROPERTIES OF MATERIALS CONTAINING LIGNIN ESTERS

In this chapter, the adsorptive properties of the new systems based on XG, lignin esters and CL are presented. Montmorillonite, a layered mineral clay with a surface covered in long hydrocarbon chain quaternary ammonium groups, has been added to the polymeric matrix with the aim of improving the materials properties, making them hydrophobic.

8.1. Materials obtainment

A schematic representation of the materials obtainment is found in the **Scheme 5**.

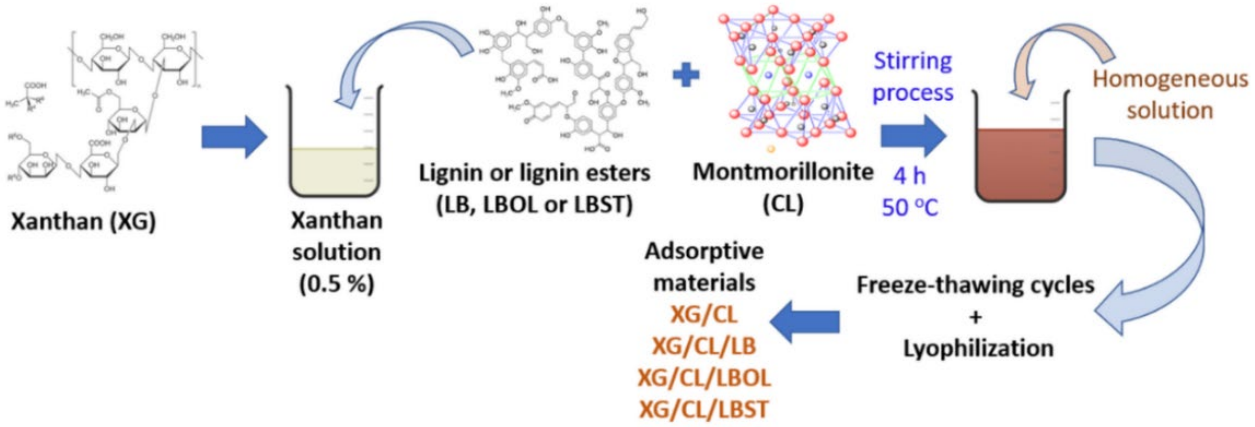

Scheme 5. Schematic representation of the materials obtainment

8.2. Materials characterization

Materials morphology

SEM images of the materials are shown in **Figure 15**. It can be observed that all of them present pores with various shapes and sizes. These structures facilitate the migration of adsorbate molecules into the pores within the materials.

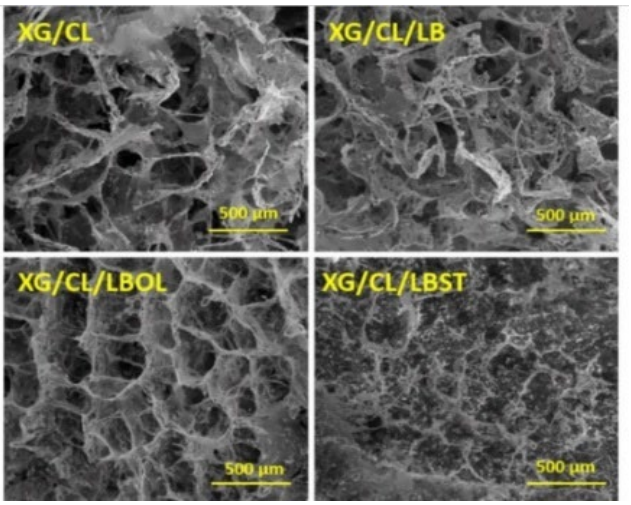

Figure 15. SEM images of materials

Compressive strength of materials

All the materials withstand deformations of over 80% without displaying structural degradation (**Table 7**). The materials exhibited different mechanical performances depending on the presence of LB or its esters. With the addition of LBST, both compressive strength and elastic modulus increased from 211.11 kPa and 4.35 kPa (XG/CL) to 287.43

kPa and 16.81 kPa (XG/CL/LBST), indicating a transition from an elastic network to a denser and more rigid one, a result that can be associated with changes in internal morphology (see SEM images, **Figure 15**).

Table 7. Compressive nominal stress, strain and compressive elastic modulus values of materials

Material	Compressive nominal stress, kPa	Strain, %	Compressive elastic modulus, kPa	R^2
XG/CL	211.11	96.96	4.35	0.997
XG/CL/LB	171.15	95.40	1.69	0.968
XG/CL/LBOL	198.16	94.43	3.19	0.996
XG/CL/LBST	287.43	97.92	16.81	0.992

The values of the deformations sustained by the materials (96.96% for XG/CL, 95.40% for XG/CL/LB, 94.43% for XG/CL/LBOL, and 97.92% for XG/CL/LBST) confirm their high mechanical strength.

8.3. Oils adsorption studies

In **Table 8** are presented the adsorption capacity values of the materials. It can be observed that both oils were retained in large quantities by XG/CL/LBOL and XG/CL. Over 75% of the total oil quantity was retained by XG/CL/LBOL and XG/CL. The adsorption process was fast, reaching equilibrium within 120 seconds. This rapid saturation of the systems with oil can be correlated with their high porosity (Wu et al., 2023).

Table 8. Materials adsorption capacity

Material	[a]q_e ± SD (g/g)					
	Argan oil			Sunflower oil		
	1 g	2 g	3 g	1 g	2 g	3 g
XG/CL	34.34 ± 9.82	40.46 ± 5.56	40.81 ± 2.39	38.34 ± 4.84	43.33 ± 0.56	51.73 ± 1.75
XG/CL/LB	29.16 ± 4.58	26.73 ± 3.11	24.50 ± 2.11	26.86 ± 1.32	32.40 ± 2.45	36.00 ± 0.36
XG/CL/LBOL	32.51 ± 1.59	42.08 ± 0.57	44.00 ± 1.38	38.06 ± 3.92	44.99 ± 3.82	46.65 ± 4.41
XG/CL/LBST	21.53 ± 2.86	32.81 ± 3.72	38.8 ± 2.36	28.92 ± 5.56	31.89 ± 1.26	32.67 ± 2.41

[a] Data are expressed as the mean ± standard deviation (n = 3)

Kinetic study

The experimental data correlate with the PSO model (R^2 values ranging from 0.9757 to 1.0000). Given the versatility of the PSO model and the nonpolar nature and significant molecular size of the oil constituents, it is expected that the interactions between the components of the systems (material and oil) are of a physical nature. The analysis of the FTIR spectra of the oil-loaded systems did not reveal the formation of new chemical bonds between the degraded oil molecules and the other components of the materials. Therefore, it can be concluded that the adsorption process is of a physical nature.

Materials reusability

The XG, LB and lignin ester-based materials (presented in **Chapter 7**) could not be washed and reused. This study confirms that the addition of montmorillonite into the polymeric matrices plays an important role in the reusability capacity of the materials. The results obtained have shown that the XG/CL and XG/CL/LBOL materials exhibit the highest oil adsorption capacity in the first cycle (**Figure 16**). This behavior can be attributed to the deterioration of the materials structure after the washing process or to the residual oil retained in their pores (Elmaghraby et al., 2022).

Future investigations will allow the optimization of the systems' composition to increase the efficiency of adsorption degraded oils.

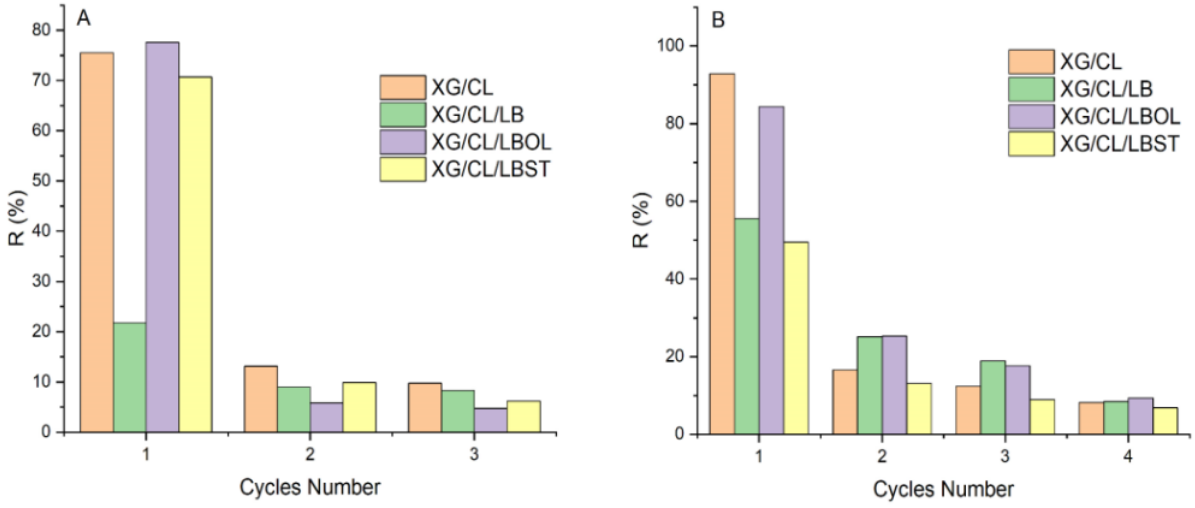

Figure 16. The reuse efficiency of studied materials for A) argan oil and B) sunflower oil

General conclusions

The analysis of the results has allowed us to draw the following conclusions:

1. Obtaining of materials based on XG, XGAC and CF for dye retention.

The esterification reaction of XG with acrylic acid was performed to reduce its hydrophilic character. The materials comprising XG esterified with acrylic acid presented superior sorption capacity and higher specific surface area as compared to XG-based systems. CF was synthesized using the co-precipitation method. It was incorporated into matrices of XG and XGAC. Adsorption experiments showed that contact time, initial concentration of solutions and temperature greatly influenced the retention process of the MB and BF dyes. XGCF and XGACCF exhibited the highest adsorption capacity (an average of 65 mg/g) and the amount of adsorbed dye increased with contact times. Furthermore, materials containing XGAC exhibited excellent adsorptive properties for the BF dye. The obtained results confirm the potential of the developed materials for wastewater treatment.

2. Synthesis of new CF–lignin hybrid materials by sol–gel auto combustion method, using LB and LO as chelating-fuel agents.

CF–LB500, CF–LB900, CF–LO500, and CF–LO900 hybrids were synthesized using the sol–gel method. Calcination was carried out at two different temperatures (500 and 900°C) to evaluate the influence of this parameter on the properties of the final products. The main advantage highlighted in this study is related to low cost of hybrids obtainment as compared to other methods, as the lignin used in the experiments is a by-product from the pulp industry.

3. The use of CF-lignin hybrids to obtain novel materials with adsorptive properties.

Materials with adsorptive properties were obtained by incorporating the hybrids synthesized at 500°C into XG and XGAC matrices. The hybrids exhibited the highest adsorption capacity for the MB dye (44.73 and 37.54 mg/g), while BF was retained in large quantities by the XG/CFLO and XG/CFLB materials (36.23 and 33.33 mg/g). The retention process of the dyes is shorter when hybrid materials are used. Both hybrids could be regenerated and reused.

4. Synthesis of lignin esters using an environmentally friendly method.

LB was esterified with oleic and stearic acids through an enzymatically catalyzed reaction. This represents one of the very first approaches in lignin chemistry. The structural differences between lignin and its esters were highlighted using various characterization methods (FTIR, ^{13}C-NMR, and XPS).

5. The use of lignin esters in XG matrices for the production of new materials with adsorptive properties.

The previously obtained lignin esters were utilized in the production of new materials with adsorptive properties. Compression strength tests showed that these materials exhibited elastic behavior. All materials retained over 50 g/g of degraded argan and sunflower oils. The adsorption process was fast, reaching equilibrium within 120 seconds.

6. Montmorillonite influence on materials with adsorptive properties.

The presence of montmorillonite led to the materials with more organized structures, exhibiting transition from an elastic to a denser and more rigid network. Studies of oils retention highlighted that the adsorption process was fast, with equilibrium reached within 120 seconds. The XG/CL and XG/CL/LBOL materials retained over 75% of the total oil content. One of the main advantages of using CL lies in the ability to reuse the obtained materials.

By integrating methods for obtaining CF-lignin hybrids, enzymatic lignin esterification and the development of cost-effective materials for an efficient adsorption of dyes and degraded oils, this work significantly contributes toward innovative, environmentally friendly, and economically viable solutions for the current environmental protection challenges.

The original results in this thesis have been published in four ISI-indexed articles (cumulative IF = 21.3), one poster and seven oral communications presented at national and international events.

Results dissemination

Papers published in ISI journals (results included in the thesis)

1. **Apostol I.**, Anghel N., Dinu M.V., Ziarelli F., Mija A., Spiridon I., An eco-friendly strategy for preparing lignin esters as filler in materials for removal of argan oil and sunflower oil, React. Funct. Polym. 190 (2023) 105620. https://doi.org/10.1016/j.reactfunctpolym.2023.105620 (IF: 5.1 – Q2 conform AIS; Q1 conform IF)
2. **Apostol I.**, Anghel N., Doroftei F., Bele A., Spiridon I., Xanthan or esterified xanthan/cobalt ferrite-lignin hybrid materials for methyl blue and basic fuchsine dyes removal: equilibrium, kinetic and thermodynamic studies, Mater. Today Chem. 27

(2023) 101299. https://doi.org/10.1016/j.mtchem.2022.101299 (IF: 7.3 – Q2 conform AIS; Q1 conform IF)

3. Spiridon I., **Apostol I.**, Anghel N.C., Zaltariov M.F., Equilibrium, kinetic, and thermodynamic studies of new materials based on xanthan gum and cobalt ferrite for dye adsorption, Appl. Organomet. Chem. (2022) e6670. https://doi.org/10.1002/aoc.6670 (IF: 3.9 – Q2 conform AIS; Q2 conform IF)
4. Spiridon I., Dascalu I.-A., Coroaba A., **Apostol I.**, Palamaru M.N., Iordan A.R., Borhan A.I., Synthesis and characterization of new ferrite-lignin hybrids, Polymers. 13 (2021) 2495. https://doi.org/10.3390/polym13152495 (IF: 5.0 – Q1 conform AIS; Q1 conform IF)

Papers published in ISI journals (results which are not included in the thesis)

1. Anghel N., **Apostol I.**, Dinu M.V., Dimitriu C.D., Spiridon I., Verestiuc L., Xanthan-based materials as a platform for heparin delivery. Molecules 28 (2023) 2757. https://doi.org/10.3390/molecules28062757 (IF: 4.6 – Q2 conform AIS; Q2 conform IF)

Participation at national and international scientific conferences (results included in the thesis)

a) Oral communications

1. **Irina Apostol**, Adina Coroaba, Iuliana Spiridon, Degraded sunflower oil adsorption onto natural-polymers–based materials, PhD Students' Days (3th edition), UAV Arad (Romania), May 2023
2. **Irina Apostol**, Maria Valentina Dinu, Narcis Anghel, Iuliana Spiridon, Xanthan and lignin esters – based materials for degraded argan oil sorption, NeXT-Chem" Innovative Cross-Sectorial Technologies" (5th edition), ICECHIM Bucharest (Romania), May 2023
3. **Irina Apostol**, Narcis Anghel, Florica Doroftei, Iuliana Spiridon, Natural polymers-based materials as adsorbents for anionic dyes, Scientific communications session of young researchers, Macro Youth (3th edition), ICMPP Iași (Romania), November 2022
4. **Irina Apostol**, Adrian Bele, Iuliana Spiridon, Cationic dye removal using materials based on xanthan or esterified xanthan/cobalt ferrite-lignin hybrid, PRIOCHEM

"Priorities of Chemistry for a Sustainable Development", (18th edition), ICECHIM, București (Romania), October 2022

5. **Irina Apostol**, Iuliana Spiridon, Narcis-Cătălin Anghel, Mirela-Fernanda Zaltariov, Thin films based on xanthan and cobalt ferrite for Methyl Blue adsorption, NeXT-Chem" Innovative Cross-Sectorial Technologies" (4th edition), ICECHIM Bucharest (Romania), May 2022
6. **Irina Apostol**, Narcis Anghel, Iuliana Spiridon, Xanthan acrylate/cobalt ferrite material for removing dyes from wastewaters, Scientific communications session of young researchers, Macro Youth (2nd edition), ICMPP Iași (Romania), November 2021
7. **Irina Apostol**, Narcis Anghel, Iuliana Spiridon, New xanthan-Co ferrite materials for removal of dyes from wastewater, Scientific communications session of young researchers, Macro Youth (1st edition), ICMPP Iași (Romania), November 2020

b) Posters

1. **Irina Apostol**, Ioan-Andrei Dascalu, Adina Coroaba, Iuliana Spiridon, Lignin as source of new hybrid materials, International Conference Progress in Organic and Macromolecular Compounds (28th edition) ICMPP Iași (Romania), October 2021

Participation at international scientific conferences/Webinar (results which are not included in the thesis)

1. **Irina Apostol**, Alexandra Dimofte, Narcis-Cătălin Anghel, Maria Valentina Dinu, Iuliana Spiridon, Alginate and xanthan-based materials used in the transdermal delivery of ketoconazole, NeXT-Chem" Innovative Cross-Sectorial Technologies" (4th edition), ICECHIM Bucharest (Romania), May 2022
2. Gianluca Colombo, Eda Yildiz, **Irina Apostol**, Namrata Pathak, Zeynep Gunes, Milena Corredig, Salvador Ruiz de Maya, Sustainability communication in food packaging: recent developments for packaged soups, COST ACTION 19124 Circul-a-bilty Webinar, April 2022

Training courses

"Sustainable food packaging design: Consumer behaviour studies" (ONLINE), European Cooperation in Science and Technology, Action 19124, Circul-a-bility, August–November 2021

Selective bibliography

- Anghel N., Dinu M.V., Doroftei F., Spiridon I., Xanthan matrix as drug delivery system, Rev. Chim. 72(1) (2021) 90. https://doi.org/10.37358/RC.21.1.8406
- Bendini A., Cerretani L., di Virgilio F., Belloni P., Bonoli–Carbognin M., Lercker G., Preliminaru evaluation of the application of the FTIR spectroscopy to control the geographic origin and quality of virgin olive oils, J. Food Qual. 30(4) (2007) 424. https://doi.org/10.1111/j.1745-4557.2007.00132.x
- Bridson J.H., van de Pas D.J., A. Fernyhough, Succinylation of three different lignins by reactive extrusion, J. Appl. Polym. Sci. 128(6) (2012) 4355–4360. https://doi.org/10.1002/app.38664
- Chandarana H., Senthil K.P., Seenuvasan M., Anil K.M., Kinetics, equilibrium and thermodynamic investigations of methylene blue dye removal using *Casuarina equisetifolia* pines, Chemosphere. 285 (2021) 131480. https://doi.org/10.1016/j.chemosphere.2021.131480
- Damacena N.K.S., Pardini L.C., Purification and characterization methods for lignin biomass as a potential precursor for carbon materials, Cellulose Chem. Technol. 53 (2019) 227–242. https://doi.org/10.35812/CelluloseChemTechnol.2019.53.23
- Elmaghraby N.A., Omer A.M., Kenawy ER., Gaber M., El Nemr A., Fabrication of cellulose acetate/cellulose nitrate/carbon black nanofiber composite for oil spill treatment, Biomass Conv. Bioref. (2022). https://doi.org/10.1007/s13399-022-03506-w
- Gandhi N.N., Patil N.S., Sawant S.B., Joshi J.B., Wangikar P.P., Mukesh D., Lipase-catalyzed esterification, Catal. Rev. 42(4) (2000) 439–480. https://doi.org/10.1081/CR-100101953
- Guo Q., Amendola E., Lavorgna M., Li Z., Feng H., Wu Y., Fei G., Wang Z., Xia H., Robust and recyclable graphene/chitosan composite aerogel microspheres for adsorption of oil pollutants from water, Carbohydr. Polym. 290 (2022) 119416. https://doi.org/10.1016/j.carbpol.2022.119416
- Hu Q., Zhang Z., Application of Dubinin–Radushkevich isotherm model at the solid/solution interface: a theoretical analysis, J. Mol. Liq. 277, (2019) 646–648. https://doi.org/10.1016/j.molliq.2019.01.005

- Kalam S., Abu-Khamsin S.A., Kamal M.S., Patil S., Surfactant adsorption isotherms: A Review, ACS Omega. 6(48) (2021) 32342–32348. https://doi.org/10.1021/acsomega.1c04661
- Kocheva L.S., Karmanov A.P., Kuz'min D.V., Dalimova G.N., Lignins from annual grassy plants, Chem. Nat. Compd. 47 (2011) 792–795. https://doi.org/10.1007/s10600-011-0061-8
- Plazinski W., Rudzinski W., Plazinska A., Theoretical models of sorption kinetics including a surface reaction mechanism: A review, Adv. Colloid Interface Sci. 152 (1–2) (2009) 2–13. https://doi.org/10.1016/j.cis.2009.07.009
- Ramadoss R., Subramaniam D., Removal of divalent nickel from aqueous solution using blue-green marine algae: adsorption modeling and applicability of various isotherm models, Sep. Sci. Technol. (2018) 1–9. https://doi.org/10.1080/01496395.2018.1526194
- Saad M., Tahir H., Ali D., Green synthesis of Ag-Cr-AC nanocomposites by *Azadirachta indica* and its application for the simultaneous removal of binary mixture of dyes by ultrasonicated assisted adsorption process using response surface methodology, Ultrason. Sonochem. 38 (2017) 197–213. https://doi.org/10.1016/j.ultsonch.2017.03.022
- Sharma P., Hussain N., Borah D.J., Das M.R., Kinetics and adsorption behavior of the Methyl Blue at the graphene oxide/reduced graphene oxide nanosheet–water interface: A comparative study, J. Chem. Eng. Data. 58(12) (2013) 3477–3488. https://doi.org/10.1021/je400743r
- Spiridon I., Apostol I., Anghel N, Zaltariov M.F., Equilibrium, kinetic, and thermodynamic studies of new materials based on xanthan gum and cobalt ferrite for dye adsorption, Appl. Organomet. Chem. (2022) e6670. https://doi.org/10.1002/aoc.6670
- Tian X., Zhu H., Meng X., Wang J., Zheng C., Xia Y., Xiong Z., Amphiphilic calcium alginate carbon aerogels: broad-spectrum adsorbents for ionic and solvent dyes with multiple functions for decolorized oil–water separation, ACS Sustainable Chem. Eng. 8 (2020) 12755. https://doi.org/10.1021/acssuschemeng.0c00129
- Wang Y., Liu S., Wang Q., Fu X., Fatehi P., Performance of polyvinyl alcohol hydrogel reinforced with lignin-containing cellulose nanocrystals, Cellulose. (2020). https://doi 10.1007/s10570-020-03396-z

- Wei S., Kamali A.R., Waste plastic derived Co_3Fe_7/$CoFe_2O_4$@carbon magnetic nanostructures for efficient dye adsorption, J. Alloys Compd. 886 (2021) 161201. https://doi.org/10.1016/j.jallcom.2021.161201
- Wu J., Ma X., Gnanasekar P., Wang F., Zhu J., Yan N., Chen J., Superhydrophobic lignin-based multifunctional polyurethane foam with SiO_2 nanoparticles for efficient oil adsorption and separation, Sci. Total Environ. 860 (2023) 160276. https://doi.org/10.1016/j.scitotenv.2022.160276
- Yue X., Liu P., Ning Y., Xu Y., Upgrading poly (butylene succinate)/wood fiber composites by esterified lignin, Compos. Interfaces. 23 (2016) 873–885. https://doi.org/10.1080/09276440.2016.1175189
- Zhu X., Tian Y., Li F., Liu Y., Wang X., Hu X., Preparation and application of magnetic superhydrophobic polydivinylbenzene nanofibers for oil adsorption in wastewater, Environ Sci Pollut. Res. 25 (2018) 22911–22919. https://doi.org/10.1007/s11356-018-2385-4